Available online at www.sciencedirect.com
SCIENCE DIRECT®
Journal of Sound and Vibration 291 (2006) 902–931
JOURNAL OF SOUND AND VIBRATION
www.elsevier.com/locate/jsvi

Numerical study of vibration damping, energy and energy flow in a beam–plate system

G. Pavić*

Laboratoire Vibrations-Acoustique, Institut National des Sciences Appliquées de Lyon, 20, avenue Albert Einstein, 69621 Villeurbanne, France

Received 19 December 2003; received in revised form 20 May 2005; accepted 4 July 2005
Available online 12 September 2005

Abstract

A full analytical model of a beam–plate system has been produced in order to study the distribution of vibration energy and energy flow in beams and rods under simple but realistic excitation conditions. Axial and flexural vibrations are only analysed. Using the developed model as well as energy formulae presented in a companion paper some characteristic features of energy distribution in thin beams/rods have been identified which can be considered as universally applicable. It has been found that axial vibrations, often neglected, may be of the same importance with respect to energy and energy flow as flexural vibrations. Moreover, axial beam vibrations may provide an efficient mechanism of energy transfer to the adjacent sub-systems. Realistic boundary conditions may result in wave conversion which in turn may reverse the flow of energy of either axial or flexural vibration toward the source. The frequency-averaged net power consumed by the beam sub-system was found to depend largely on damping, contrary to the total input power to the system which stays fairly insensitive to it. The energy sharing between the beam and the connected plate was found to depend little on the amount and distribution of damping within the system providing the coupling between the two is strong. Finally, simulation of measurements of energy flow as well as of absorption/reflection/transmission energy coefficients of incorporated joints was shown to be affected to a large degree by beam damping which is often disregarded in experimental work.

*Tel.: +33 472438707; fax: +33 472438712.
E-mail address: pavic@lva.insa-lyon.fr.

0022-460X/$ - see front matter © 2005 Elsevier Ltd. All rights reserved.
doi:10.1016/j.jsv.2005.07.020

1. Introduction

Rods and beams are some of the simplest components of mechanical structures. The earliest investigations on the propagation of mechanical energy in structures were carried out precisely on these components. Yet, even at moderate frequencies at which simple rod and beam vibration models are satisfactory the analysis of energy propagation, either by computation or measurement, remains a problem. Simplified theories of energy distribution were successful in dealing with axially vibrating rods, but less successful in dealing with beams vibrating in flexure. Measurement techniques have not yet left laboratory conditions and, even so, the results are often not convincing. As a rule, the structural damping, being rather difficult to handle, is neglected in measurements.

The main objective of this paper and its companion paper [1] is to contribute to the understanding of some basic features of energy distribution and flow in rods and beams. While the first paper deals with some generic notions of energy via an analysis of semi-infinite structures, this paper will be focused on a finite rod/beam. The drawback in dealing with a finite system is that the results have to loose generality in favour of detail such as boundary conditions. The study will therefore be conducted in the spirit of ''demonstrating effects'' rather than formulating generalised conclusions.

Reference to measurement and modelling will be made where appropriate. The distinction will be made between kinetic and potential energy. The former is usually associated with adverse effects of vibration on humans, while the latter is responsible for dissipation effects in structurally damped systems as shown in Ref. [1] or with mechanical damage. Thus potential energy can serve as an indicator of the locations of high damping effect and thus can be used in vibration control optimisation.

The terms ''rod'' and ''beam'' are usually employed to make a distinction between axial and flexural vibrations. Experience shows that these two types of vibration often coexist. One of the objectives of the current paper is to make an account of such a coexistence where energy is concerned. This will be done by modelling a single mechanical object, a beam, which will be subjected to both axial and flexural vibration. In order to make a realistic but not too complex model, the beam is taken free at one end and fixed to a plate at the other end. Such a configuration is suitable because it will lead to natural wave conversion at the connection point. Thus even in the case of single excitation type, either axial or flexural, both longitudinal and flexural waves will be generated in the beam. The energy induced by both types of motion will be investigated.

2. Characteristics of a beam–plate system

The structure selected consists of a straight beam connected perpendicularly to a flat plate. This structure will be modelled in order to analyse the influence of damping on energy characteristics of the beam and to carry out numerical experiments using the energy formulations developed in Ref. [1].

2.1. Beam–plate model

The beam is made of steel, the dimensions are: length—2 m, radius of inertia—1 cm, mass per unit length—2 kg/m. It is attached to a $0.5\,\mathrm{m} \times 0.42\,\mathrm{m}$ 10 mm thick steel plate. These values are

typical of standardised elements in mechanical design. For example a steel pipe of 30 mm diameter and 3 mm thickness used a lot in gas and liquid transport installations will have these parameters, while 10 mm is a standardised thickness for steel sheets used in general construction works. The plate thickness was chosen such that the flexural driving point impedances of the beam and plate are of comparable average values. The excitation acts in a single point of the beam placed at a distance 0.5 m form the free end; Fig. 1. The junction position on the plate, chosen at random, is 0.29 m length wise, 0.22 m width wise. The beam and the plate materials are assumed to be identical: Young's modulus 2×10^{11} Pa, mass density 7800 kg. The reference value of loss factor is 1%; this value will occasionally be varied where appropriate. In this study the realism of the model matters which explains the attention paid to the choice of model parameters.

The plate is taken simply supported along all the edges. While the plate boundary conditions are fairly irrelevant in this study, the supported boundary conditions offer the advantage of enabling straightforward analytical computation of plate response. The excitation is assumed to come from a rotating unbalanced mass m of eccentricity e positioned at a distance $d = 10$ cm away from the beam axis. Under such an excitation the beam will be subjected to an axial force N, a lateral force F and a bending moment M which, in complex notation, read:

$$N = Q\mathrm{e}^{\mathrm{j}\omega t}, \quad F = -\mathrm{j}Q\mathrm{e}^{\mathrm{j}\omega t},$$
$$M = Nd = Qd\mathrm{e}^{\mathrm{j}\omega t}, \quad Q = me\omega^2. \tag{1}$$

The simplicity of the beam–plate model will be further enhanced by assuming that the beam–plate junction couples the movements in the vertical plane only. Such a type of junction could theoretically be manufactured, but it has no value from the design point of view. It is used here for the sole purpose of making the beam vibrate in the vertical direction only which will simplify the presentation of results without affecting the objective of coupling axial and flexural movements.

The response will be analysed as a function of rotation frequency ω. In order to avoid excessive increase of excitation at high frequencies, the value of centrifugal force Q will be kept unitary.

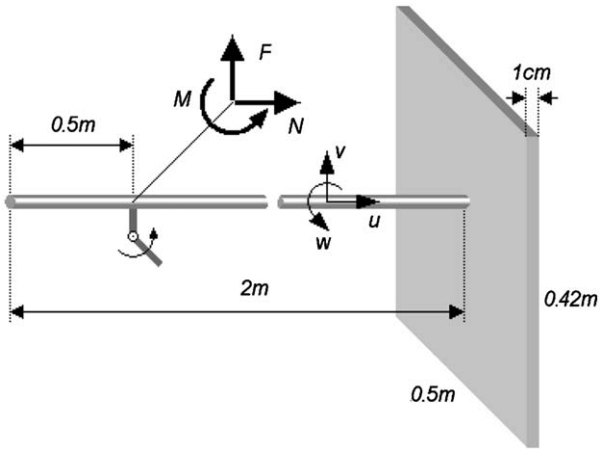

Fig. 1. Beam–plate system. Simultaneous axial, lateral and bending excitation is provided by an eccentric rotating mass.

This simplification in no way affects the analysis and the findings. In the other hand the frequency variations of energy quantities, proportional to excitation square, will be easier to follow if the frequency weighting of excitation is suppressed. The original phases between N, F and M will be conserved though.

The axial beam motion is modelled by the thin-rod theory starting with the closed form mobility solution of a free–free rod excited at one end. Two free–free sections are then coupled across the (external) driving force to provide the mobility of a free–free rod for an arbitrary pair of excitation and response positions. A similar procedure is employed to obtain the response of a free–free beam subjected to a force or a moment excitation. The flexural beam motion is modelled by Euler–Bernoulli theory. The beam axial and flexural response are obtained using direct resolution of rod and beam wave equations rather than using modal summation. The plate is modelled in a classical way by a real-mode superposition [2].

Once the general beam model was made, the connectivity between the beam and the plate was taken into account by assuming that the plate in-plane impedance was much higher than the beam flexural impedance. The plate in-plane impedance was estimated using an expression found by Nikiforov, [3], obtained by considering an in-plane force acting on an infinite plate via a circular indenter. Given the dimensions of beam cross-section and plate thickness the assumption about the plate impedance was judged to be realistic. In this way the coupling movement at the connection point consisted of beam axial movement and rotation only since the transversal beam movement was effectively blocked by the plate.

The model of the beam–plate system is outlined in the Appendix. It provides the complex amplitudes of two longitudinal and four flexural waves in each of the two sections of the beam. The values of wave amplitudes are used to compute the energy and energy flow using the equations of Ref. [1].

2.2. Global energy characteristics

The beam and the plate, taken individually, exhibit characteristic multi-resonant behaviour. Fig. 2 shows the average global RMS vibration level of the free-blocked beam (a) and plate (b) under unit excitation. The excitation position of the beam is the same as specified before, that of the plate is at the connection point. The resonant peaks are well separated. The simplified theoretical values of modal density, equal to $0.112f^{-1/2}$/Hz (beam, flexure), 0.0012/Hz (beam, axial), and 0.00687/Hz (plate, flexure), indicate fairly low modal overlap at 1% loss factor.

Fig. 3 shows global power characteristics of the system analysed. Fig. 3(a) shows the total net power supplied by the external excitation (full line) and the power transmitted to the plate (dashed line). As the two curves overlap close to resonant peaks, markers are employed to improve visibility. It can be seen that at some resonant frequencies, the 4th 7th 10th 12th, etc., some significant input power is transmitted to the plate which dissipates more energy than does the beam. Fig. 3(b) shows how the power consumed by the beam, i.e. the difference between the input power and power supplied to the plate, is contributed by axial and flexural excitations.

In the presently analysed case the flexural excitation globally consumes more energy, but at some frequencies the energy consumed by axial motion becomes larger. This is notably the case around the resonant frequency at 162 Hz. The phenomenon is not related to the ''local'' beam resonance; the lowest blocked beam resonance is at $\approx$600 Hz, Fig. 2(b), implying that in free–free

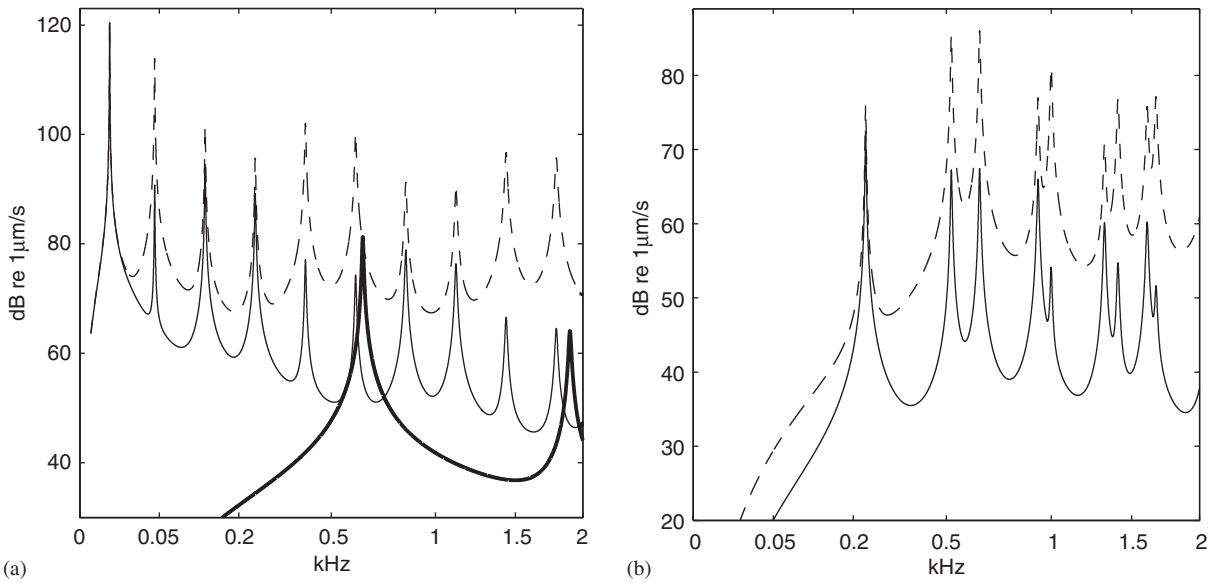

Fig. 2. rms vibration level of system components in under unit excitation: (a) free–clamped beam; (b) plate. Full line, normal force; dashed line, moment in vertical plane; thick line, axial force.

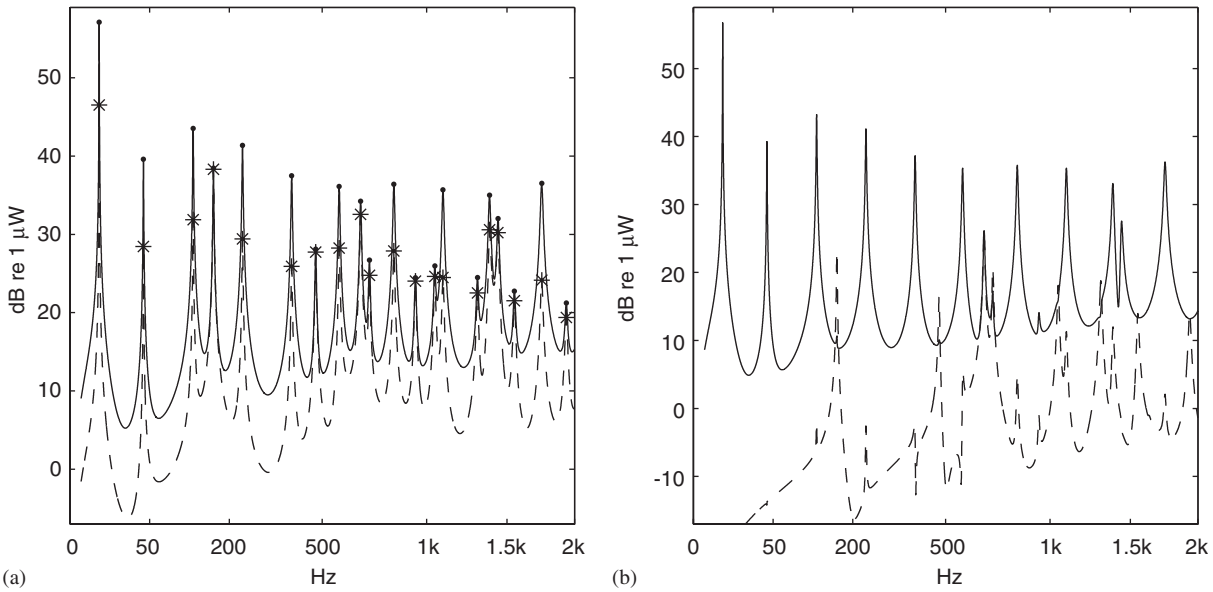

Fig. 3. Global net power in the system: (a) full line, input power; dashed line, power delivered to the plate; (b) power consumed by the beam: full line, supplied by lateral force and bending moment; dashed line, supplied by axial force. Markers indicate system resonant frequencies.

conditions the lowest resonance is twice that high. In fact, the mass of the beam coupled to the stiffness-controlled sub-resonant plate creates a system resonance at 162 Hz. The whole system behaves at this frequency as a lumped parameter mass–spring vibrator. The large connection force

acting in parallel with correspondingly large inertial forces along the beam yield strong axial deformations which, in spite of the absence of beam resonance, result in an elevated energy consumption within the beam. The energy dissipation will thus sometimes be "invisible" if judged by the vibration level. At higher system resonant frequencies at which the axial vibration dissipates most of the energy in the beam the effect described is merged with the effects of axial beam resonances.

The powers consumed in the beam under axial and flexural excitations, shown in Fig. 3(b), are not equal to the powers of longitudinal and flexural vibrations though. As the two types of vibration are coupled through the plate, a purely axial excitation would produce transfer of energy flow in the beam by both axial and flexural vibrations. The same would apply to a purely flexural excitation. This is demonstrated in Fig. 4. Shown are the axial and flexural energy flows entering the connected side of the beam at the excitation point. While the power consumed by the beam is, naturally, positive at all frequencies, the two energy flows become independently negative at some frequency bands. Negative values are indicated by dashed lines.

In the preceding example the loss factors of axial and flexural vibrations were supposed identical, 1%. In reality these can be different from each other. Structural dissipation is governed by strains: in axial vibration by normal strains only and in flexural vibrations by both normal and shear strains. This results in different loss factors for the two motions. For example the loss factor of axial vibrations in aluminium is typically half of that of flexural vibrations.

Fig. 5 shows the energy consumed by the beam and the plate when the loss factors of axial and longitudinal vibrations are unequal. The loss factor of flexural vibration was held constant, 1%, that of longitudinal vibration was changed ten times, first decreased to 0.1% and then increased to

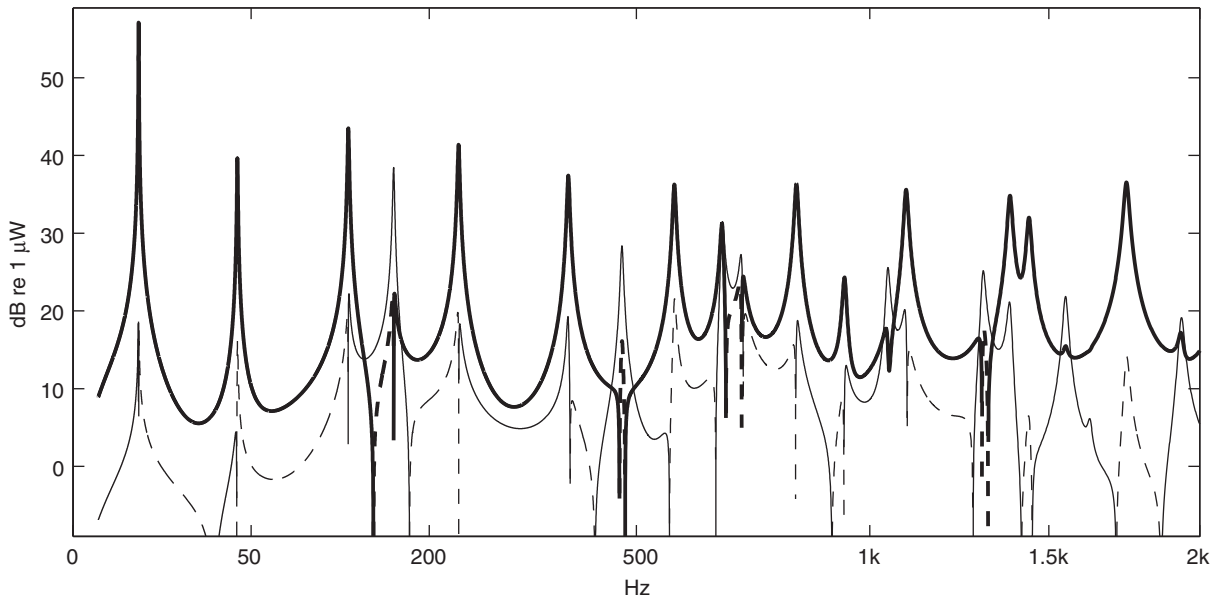

Fig. 4. Energy flow at the excitation point in the direction of connection point. — flexural; — axial. Dashed lines, negative values.

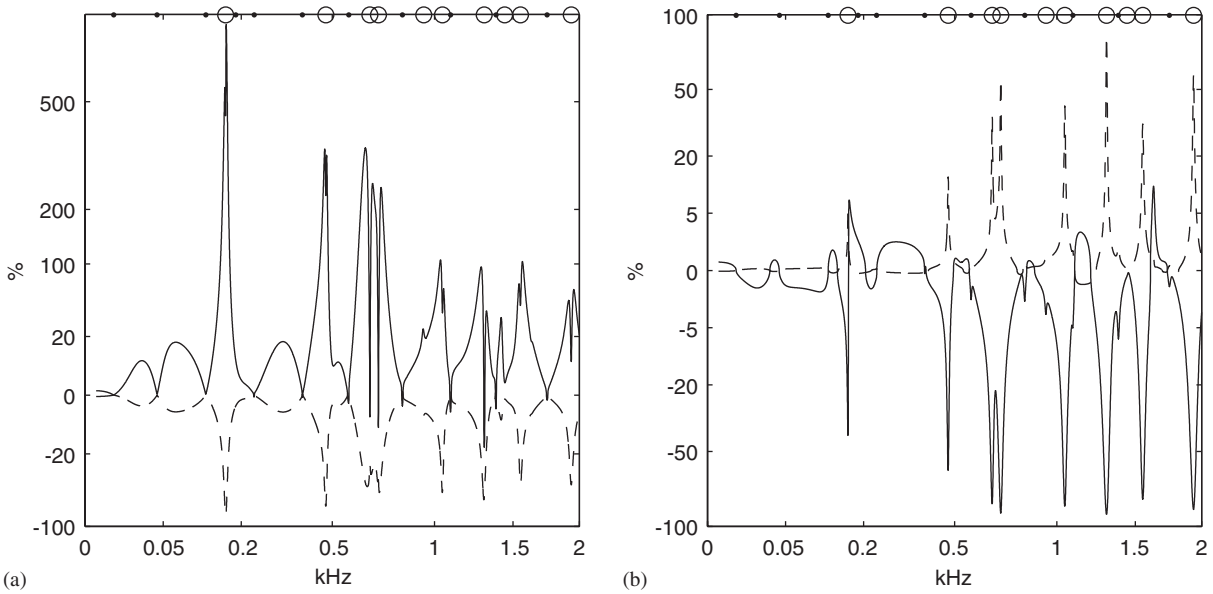

Fig. 5. Effect of non-proportional damping to energy consumed by the (a) beam and (b) plate. Curves represent the ratio of the consumed energy with modified axial damping and that with original axial damping. Axial loss factor: 0.1% (dashed line) and 10% (full line). Constant flexural loss factor, 1%.

10%. The results are displayed by dividing the power values by the power under initial conditions, (axial loss factor 1%). Square root scaling is used for improved resolution.

While the increase (decrease) of axial damping is followed by an increase (decrease) of energy consumed by the beam, the opposite is seen to apply to the plate. The plots show that the effect of changing axial damping is considerable at some narrow frequency ranges, with the response peaking at some particular frequencies. It turns out that these frequencies are the system resonances at which the plate absorbs more energy than the beam. These resonances are indicated by circles at the upper graph boundary. At the remaining resonances, indicated by dots, the effect is virtually non-existent. A closer look at the energy consumed by axial beam vibration and that supplied to the plate reveals that at the resonances dominated by the plate the energy flow entering the plate is supplied essentially by the axial beam motion which itself dissipates less energy than it transmits. This explains the inverse trends in beam and plate dissipated energies with changing the axial damping. The result is certainly relevant for vibration control of the plate which may prove inefficient if the attention, as is often the case, is focused on damping only flexural vibration of the sub-system supplying the plate energy.

It can be concluded that the analysis of energy flow in beams integrated in built-up systems should be carried out by taking into account both types of vibration, flexural and axial, the latter being often disregarded in current practice. Wave conversion may produce torsional vibration too. The coupling which generates the wave conversion can lead to energy flow carried by one type of vibration which is in the direction opposite to that of the total flow. Any simplified energy flow analysis may thus be erroneous.

2.3. Kinetic vs. potential energy

Fig. 6 shows the sharing of kinetic and potential energies in the form of a non-dimensional factor, the Lagrangian coefficient. This coefficient is defined here as the ratio between the difference of kinetic and potential energies, called the Lagrangian energy, and their sum, i.e. the total energy. The Lagrangian coefficient is thus a normalised measure of the unevenness of kinetic and potential energy sharing in the system. Fig. 6(a) shows the coefficients relative to the whole system (full line) and to the beam only (dashed line). The two look similar. At the system resonant frequencies the kinetic and potential energies are practically equal reducing the system coefficient almost to zero. Below the first system resonance at 6.8 Hz both coefficients rapidly decrease toward -1 as expected. Above the first resonance up to 100 Hz there exists one system resonance at 42.5 Hz but less strong than the first one. Below any given resonant frequency the potential energy of a given mode is higher than the corresponding kinetic energy and vice versa. Since the first mode dominates the second one in the present case while the overlap of natural frequencies of the two modes is low, the kinetic energy of the first mode will be higher than the potential energy of the second mode practically throughout the whole span between the two natural frequencies. The Lagrangian coefficient is consequently positive and large between the two resonances. The third resonance is again further apart, but is of higher level than the second one. As a consequence, the Lagrangian first rises above the second resonance but then falls below zero by approaching the third resonance. At higher frequencies the relative span between the successive resonances gets smaller and consequently the differences between the potential and kinetic energies decrease.

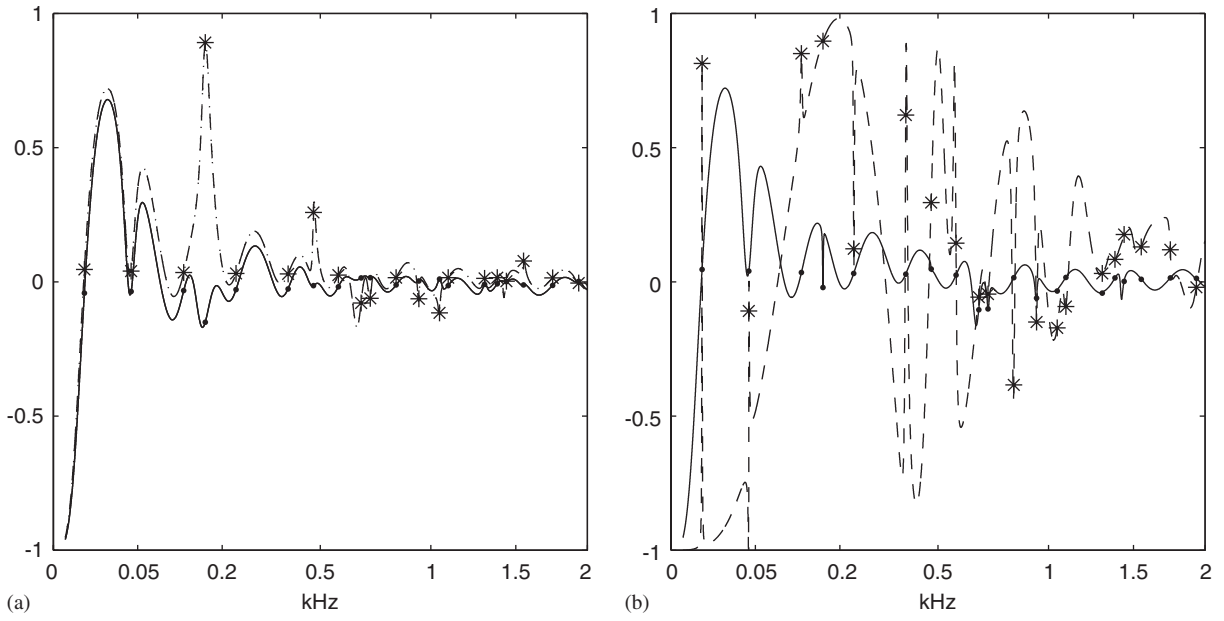

Fig. 6. Lagrangian coefficient of beam–plate system: (a) full line, whole system; dashed line, beam only; (b) full line, flexural beam vibration; dashed line, axial beam vibrations. Markers indicate positions of system resonant frequencies.

A strong peak can be noticed in the beam Lagrangian at 162 Hz and one less strong at 475 Hz. These peaks are not present in the Lagrangian of the entire system. At 162 Hz, dominated by axial motion, the beam will add about 18 times more kinetic energy than the (already elevated) potential energy. At this same frequency the kinetic and potential energies of the whole system are nevertheless almost the same. This example shows how the whole assembly, while showing a global tendency to even up the kinetic and potential energies, allows a large local mismatch of the two which results in an uneven energy loss across the system.

Fig. 6(b) shows the Lagrangian coefficients of axial and flexural vibrations of the beam. The former one exhibits strong oscillations throughout the frequency range of analysis indicating that kinetic and potential energies of axial motion are very different from each other. The latter stays close to the global Lagrangian coefficient of the beam which is understandable because the energy of flexural motion dominates overall.

It can be concluded that the kinetic and potential energies of a beam integrated in a built-up system can differ by a non-negligible amount. Furthermore, the kinetic and potential energies of either axial or flexural motion considered individually can be very different from each other.

3. Effect of damping on system energy

3.1. Damping and system energy level

Clearly, internal damping provides a key link between the power supplied to a system and its energy. The relationship between the damping and the power supplied is not straightforward though. Heckl et al. have shown that the net input power P of a point excited system is independent of damping if averaging is done in a frequency band $\Delta\omega$ containing at least several resonances and furthermore over all excitation positions, [4]:

$$P = \langle |\mathbf{F}^2| \rangle_{\Delta\omega} \frac{\pi \upsilon}{4m}, \tag{2}$$

where υ is the modal density, m the system mass. A study of two simple, conservatively coupled sub-systems has revealed that significant differences in damping types, concentrated or distributed, did not affect sub-system powers appreciably, [5].

By considering vibration of infinite and periodic waveguides under point excitation Langley has demonstrated that internal damping can considerably affect input power, [6]. He has shown that the contribution of non-resonant modes, neglected in the derivation of Eq. (2), can be important in the conditions of high modal overlap. The modal overlap, here taken as $\mu = \pi \upsilon(f) f/2$, rises with frequency as seen in Table 1. It is thus of interest to find out how damping influences sub-system energies and power transmission where a finite beam system is concerned.

The effect of damping will be analysed in two ways: (a) directly, by looking at the input power at different amount of system damping and (b) in a relative way, by looking how the distribution of damping affects the distribution of system energy.

To get an average account of the effect of damping on input power the computation will be done by averaging in frequency bands. An extended frequency range was considered, 0–5 kHz, needed to involve sufficient number of resonances for averaging. Seven different values of loss

Table 1
Modal overlap MO of beam and plate at characteristic frequencies

	50 Hz	100 Hz	200 Hz	500 Hz	1 kHz	2 kHz
Beam	0.013	0.018	0.025	0.039	0.056	0.079
Plate	0.005	0.011	0.022	0.054	0.108	0.216

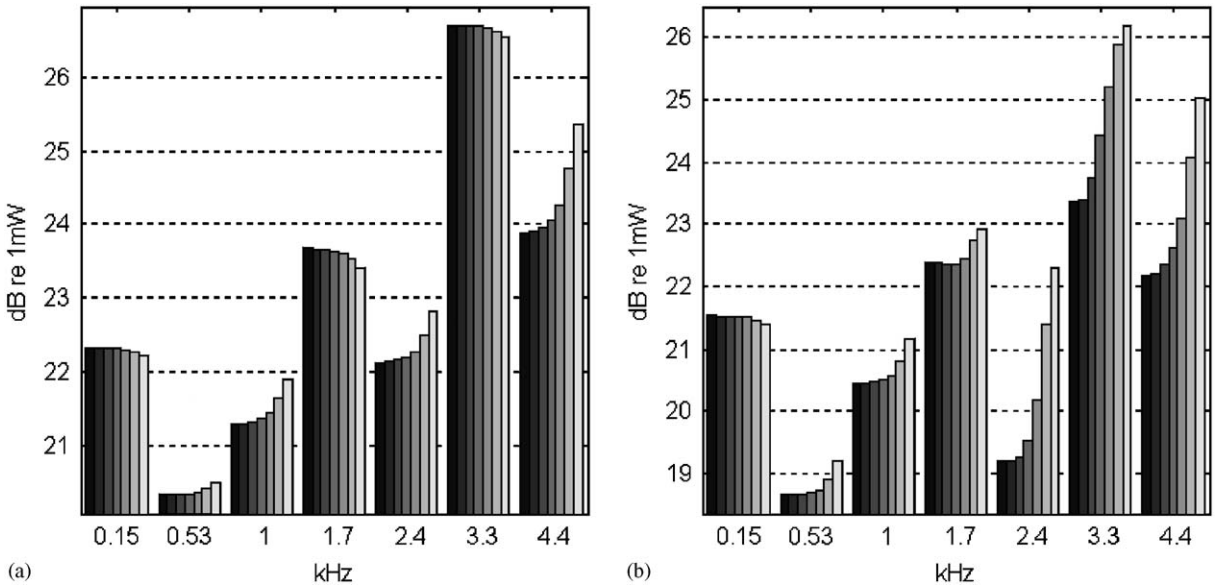

Fig. 7. Frequency-averaged net input power to the system: (a) global power supplied by the excitation; (b) power consumed in the beam. Abscissa figures represent band centre frequencies. Columns represent loss factors: 0.1%, 0.2%, 0.5%, 1%, 2%, 5%, 10%.

factors were selected: 0.1%, 0.2%, 0.5%, 1%, 2%, 5% and 10%. The results were averaged using the following sequence of bands: 0–300–750–1320–2000–2780–3880–5000 Hz. Each band contains at least five modal frequencies of the coupled system. Fig. 7 shows the averaged net input power of the beam–plate system. The plot (a) concerns the entire system while the other plot concerns beam section only. It can be seen that the input power is fairly independent of system damping where the entire system is concerned. The higher the damping the more the input power deviates from its mean value. Fig. 7(b) shows much larger power variations of the beam section than are the variations in the power of the entire system.

The beam, considered on its own, is excited at two positions: externally at the driving point and internally at the connection point. At both of these points the excitation is by a normal force, a lateral force and a bending moment. But the complexity of excitation could not have been the cause of large variation in beam power, since large power variations would have been noticeable in the values of system power too. In order to explain the increase in power variations of the beam, the exact value of the input power will be evaluated in the case of two harmonic forces of

complex amplitudes F_1 and F_2 acting simultaneously. Using modal superposition the net power can be readily expressed as a series:

$$P = \frac{\eta\omega}{2m}\sum_n \frac{\omega_n^2\left[|F_1^2|\phi_{1,n}^2 + |F_2^2|\phi_{2,n}^2 + 2\mathrm{Re}(F_1F_2^*)\phi_{1,n}\phi_{2,n}\right]}{(\omega_n^2-\omega^2)^2 - \eta^2\omega_n^4}. \tag{3}$$

Here $\phi_{1,n}$ and $\phi_{2,n}$ are the normalised eigenfunctions at the excitation points 1 and 2, ω_n the n$^{\mathrm{th}}$ eigenvalue.

Providing the forces F_1 and F_2 are of constant spectral density G_{11}, G_{22} and G_{21} within a frequency interval $\Delta\omega = \omega_b$-ω_a integration over this interval gives

$$\begin{aligned} P &= \frac{1}{4m}\sum_n \Gamma_n\xi_n, \\ \Gamma_n &= G_{11}\phi_{1,n}^2 + G_{22}\phi_{2,n}^2 + 2\mathrm{Re}\{G_{21}\}\phi_{1,n}\phi_{2,n}, \\ \xi_n &= \tan^{-1}\left(\frac{\omega_n^2-\omega_a^2}{\eta\omega_n^2}\right) + \tan^{-1}\left(\frac{\omega_b^2-\omega_n^2}{\eta\omega_n^2}\right). \end{aligned} \tag{3a}$$

The frequency-averaged input power is thus represented as a modal sum of the product between an excitation-dependent factor, Γ, and a damping-dependent factor ξ. This result can be of course generalised to an arbitrary number of excitations as Γ represents in fact modal excitation density. It holds irrespective of whether a particular eigenvalue ω_n is within or outside the integration interval but is inapplicable if the modal excitation density changes with frequency.

If the damping is very small and the eigenvalue ω_n not very close to either of the two integration limits the values of $\tan^{-1}$ will be fairly independent of damping. The damping factor ξ will then be approximately equal to π if ω_n lies within the integration interval and to zero elsewhere. An analogous result, obtained in Ref. [4] for the case of single excitation force, leads to Eq. (2) providing that averaging is done over all excitation positions. This assumption, often employed in Statistical Energy Analysis, is not applicable to the present study.

Fig. 6 shows the damping factor ξ for an octave averaging band at different values of loss factor. The abscissa is the ratio of the eigenvalue and the band centre frequency. It can be seen that the higher the damping the more ξ deviates from the 0–π–0 dependence. The leakage to eigenvalues lying outside the averaging interval becomes then non-negligible as found in Ref. [6] Fig. 8.

The excitation of the beam–plate system was taken to be independent of frequency which explains the low variation of input power with damping. The excitation of the beam within the system is however extremely dependent on frequency since the connection forces and moments acting on the beam vary a lot with frequency in a typical resonant fashion. This explains the much stronger variation of beam consumed energy with damping. More computations carried out by increasing band widths were found to produce results fully consistent with the shown ones. The effect of non-uniform excitation density cannot be removed by increasing the band width.

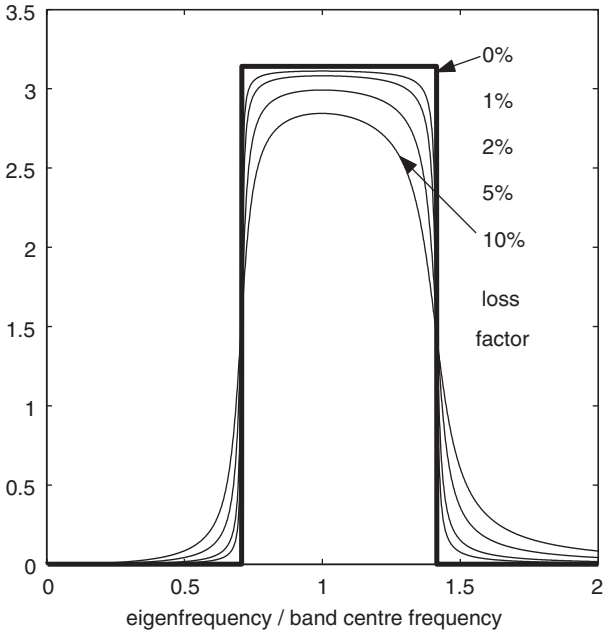

Fig. 8. Damping factor.

3.2. The influence of damping distribution on energy

The power consumed within the beam, i.e. the difference of input power and the power transmitted to the plate at the connection point, thus depends to a large extent on internal damping, even when frequency averaged, and this is irrespective of whether the excitation depends on frequency or not. The next question is about how the powers and energies of the whole system are shared by the beam and plate in dependence of damping. This question is relevant for vibration control: the efficiency of an external damping treatment used for vibration reduction depends to a large deal on its placement.

To start with, a simple system consisting of two linear point-coupled sub-systems will be analysed first. System 1 is excited by a point force. In such a case the connection force F_C is related to the excitation force F by a simple mobility ratio:

$$F_C = -\varsigma F, \quad \varsigma = \frac{M_T}{M_C}, \quad M_C = M_1 + M_2.$$

Here M_T is the transfer mobility of the system 1 between the driving and connection points, M_1 and M_2 are driving point mobilities of systems 1 and 2 at the connection points. The coupled system is at resonance when the sum of mobilities at the coupling, M_C, is at minimum. By denoting the driving point mobility at the excitation point by M_E the ratio of net powers supplied to sub-systems 1 and 2 can be easily found to be

$$\frac{\mathrm{Re}\{P_1\}}{\mathrm{Re}\{P_2\}} = \frac{\mathrm{Re}\{M_E\} - \mathrm{Re}\{\varsigma M_T\}}{\mathrm{Re}\{M_2\}|\varsigma^2|} - 1. \tag{4}$$

The terms which dominate in Eq. (4) are the real parts of mobilities at different points. The real part of mobility, either driving or transfer, increases with damping away from resonances but decreases with damping close to resonances. Providing the damping stays small, the following can be drawn from (4):

- The ς factor will increase close to a system resonance (denominator small, coupling force strong). An increase in plate damping should thus reduce the coupling force and ς will drop. The influence of beam damping should produce a similar effect, less strong though as the beam is the driven sub-system. At a beam resonance both the numerator and denominator rise, thus the influence of beam damping should not be marked. At a plate resonance ς drops with plate damping.
- The numerator in Eq. (4) contains two terms, the first of which increases at beam resonances where it becomes proportional to beam damping inverse. The second term rises at both beam and system resonances, the former inversely with beam damping. The effect of plate damping cannot be generalised, but is not strong. Away from system resonances this term rises with both beam and plate damping.
- The denominator in Eq. (4) will peak at system resonances, decreasing with beam damping and to a lesser extent with plate damping providing the beam damping is low. This term stays fairly unaffected by either the beam or plate resonances. Away from system resonances this term is almost independent of beam damping, but increases with plate damping.
- The first term in Eq. (4) represents the ratio of the powers dissipated in the beam and plate, respectively. It will be normally well above unity in absolute value providing the two sub-systems are of comparable capacity in energy storage and well coupled, as it is the case analysed. Under such conditions this power ratio will increase with the damping of the beam and decrease with that of the plate.

All taken into account, the ratio of net powers of two connected sub-systems, the first externally driven and the second passive, will be under some conditions, mentioned below, proportional to the ratio of their loss factors (beam dissipated power > plate dissipated power):

$$\frac{\mathrm{Re}\{P_1\}}{\mathrm{Re}\{P_2\}} \approx \frac{\eta_1}{\eta_2}. \tag{4a}$$

This result holds better the lower the damping and the further the frequency is from system resonances. It has been assumed that resonance effects are not being influenced by each other, in other words that the conditions of low modal overlap apply. Eq. (4a) has a major consequence on the sharing of beam and plate energies. The relationship between the complex input power to a system P and its global kinetic E_k and potential E_p energies reads, [9]:

$$\bar{P}_{\mathrm{in}} = 2\omega\left[\mathrm{j}\bar{E}_k + (\eta - \mathrm{j})\bar{E}_p\right]. \tag{4b}$$

The potential energy of the (structurally damped) beam is proportional to the ratio of the total net (real) power delivered to the beam and its loss factor. The analogous rule applies to the plate. It follows that the potential energies of the beam and plate, and thus approximately their total energies, will stay roughly in the same proportion at low modal overlap irrespectively of how the

damping is distributed between the beam and plate:

$$\frac{E_{p1}}{E_{p2}} = \frac{\mathrm{Re}\{P_1\}/(2\omega\eta_1)}{\mathrm{Re}\{P_2\}/(2\omega\eta_2)} \approx \mathrm{const} \approx \frac{E_1}{E_2}. \tag{5}$$

The result (4b) is not surprising where frequencies not close to system resonances are concerned: in any lightly damped system the response, and thus the energy, is unaffected by damping away from resonance. But Eq. (4b) hold at resonance too if the modal overlap is low as shown above. An equivalent result obtained in Ref. [4] expresses the ratio of frequency-averaged kinetic energies of two coupled sub-systems, 1 and 2, in terms of modal sub-system densities υ as well as the damping and coupling loss factor of the driven sub-system:

$$\frac{\langle E_{k2}\rangle}{\langle E_{k1}\rangle} = \frac{\upsilon_2}{\upsilon_1}\frac{\eta_{21}}{\eta_{21}+\eta_2}. \tag{6}$$

Eq. (6) follows directly from the basic SEA equation applied to two sub-systems by replacing kinetic energy by half the total energy. At low modal overlap the coupling loss factor is proportional to damping, thus Eq. (6) is effectively damping independent. With increase in overlap the coupling becomes weaker and the independence on damping is lost.

In a series of articles Mace has analysed in detail the energy of coupled one-dimensional waveguides, in particular ensemble statistics and wave coherence effects of such systems; e.g. Refs. [7,8]. A major improvement of traditional statistical power calculation was made by taking account of sub-system reflections in a simple yet efficient way. The peak power supplied to a strongly coupled system was found to occur at system resonances, as confirmed above. With the coupling decreasing the power maxima shift to sub-system natural frequencies. The strength of coupling was expressed in Ref. [8] in terms of two types of coefficients: the waveguide reflectance, equivalent to modal overlap, and the coupling transmission coefficient. High transmissibility and low overlap lead to strong coupling, which is the actual case. A beam–plate model, similar to the present one except for infinite plate size, has been used in Ref. [7] as an example. Incidentally, this model was found to produce results somewhat different than the analogous ones obtained by the present model. The differences may be explained not only by the mismatch in plate geometry but also in the treatment of the beam near field which was fully accounted for in the present model.

Fig. 9 shows the ratio of beam and plate net powers at different values of beam and plate damping. The result is presented in the form of a shaded area obtained by varying the loss factor in the beam and independently in the plate between 0.5% and 5% such that all possible combinations of the two factors were covered.

The power sharing by sub-systems crucially depends on damping. This is clearly seen in Fig. 9(a) showing the bare ratio of beam and plate powers. On the contrary the ratio of beam and plate energies shown in Fig. 9(b) is seen to be little affected by the distribution of damping. It can be demonstrated that the spread of results further reduces with reducing the maximum value of the scanned damping. In other words, at not too high values of loss factor the beam and plate energies stay roughly in the same proportion no matter how large is the damping and how unevenly is it shared between the beam and the plate. The exception to this rule is seen at some frequencies where the spread of values of the energy ratio increases as predicted by the simple model.

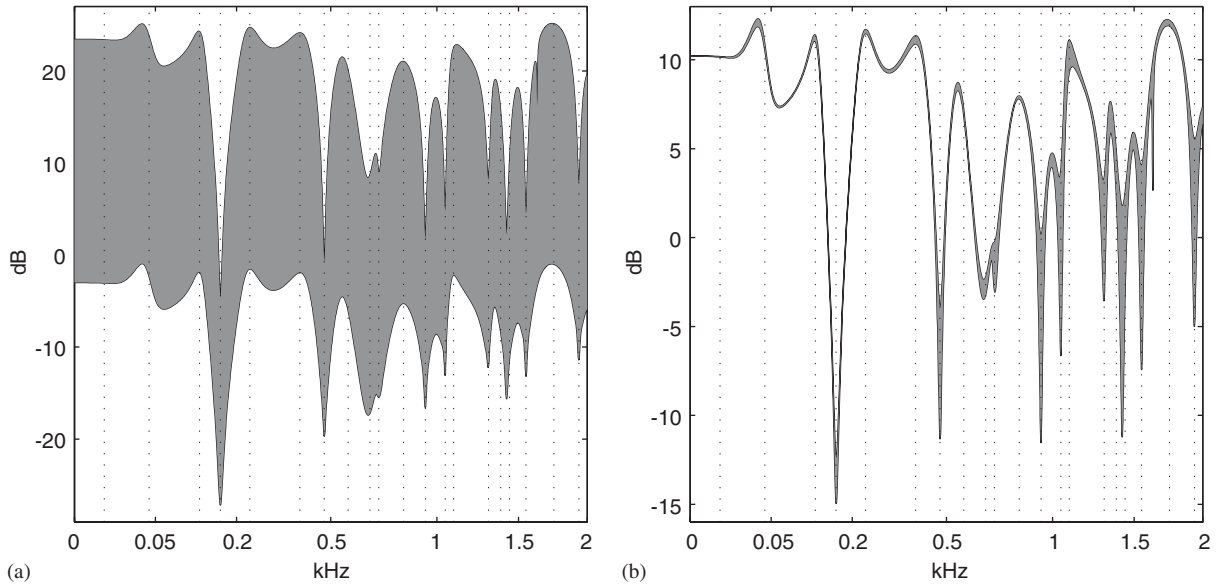

Fig. 9. Power sharing in beam–plate system under all possible variations in beam and plate loss factors between 0.5% and 5%. (a) Ratio of net powers delivered to beam and plate; (b) ratio of beam and plate energies. Dotted lines indicate positions of system resonant frequencies.

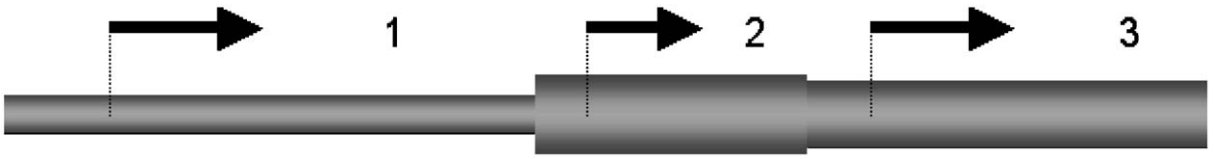

Fig. 10. Three-rod system.

It should be mentioned that the result (4a) applies to two coupled sub-systems one of which is excited. Eq. (4) does not provide justification for an extension of this result to multiple coupled sub-systems. Nevertheless, a simple example concerning a system consisting of three rods coupled in series, shown in Fig. 10, demonstrates that the independence of energy ratios on damping is still valid to an acceptable level of approximation. This can be confirmed by applying the modelling developed in Ref. [7]. In the present example all three rods are externally excited. As in the previous beam–plate case the modal overlap of the rods is low. The results are displayed in Fig. 11. The shaded areas show the variation of the ratio of the total energy of each rod and the total system energy, i.e. the sum of the three, for all possible independent variations of loss factors of each rod between 0.25% and 5%. The system parameters are shown in Table 2.

While the ratio of beam and plate energies was shown to be fairly insensitive to damping sharing between the two, the actual energy levels of course depend vitally on damping. Fig. 12 shows the plate, beam and global energy levels in dependence of beam and plate loss factors. The values are given in a normalised way, by dividing the energy with the minimum energy which was shown to correspond to maximum values of beam and the plate loss factors, i.e. 5%. The results

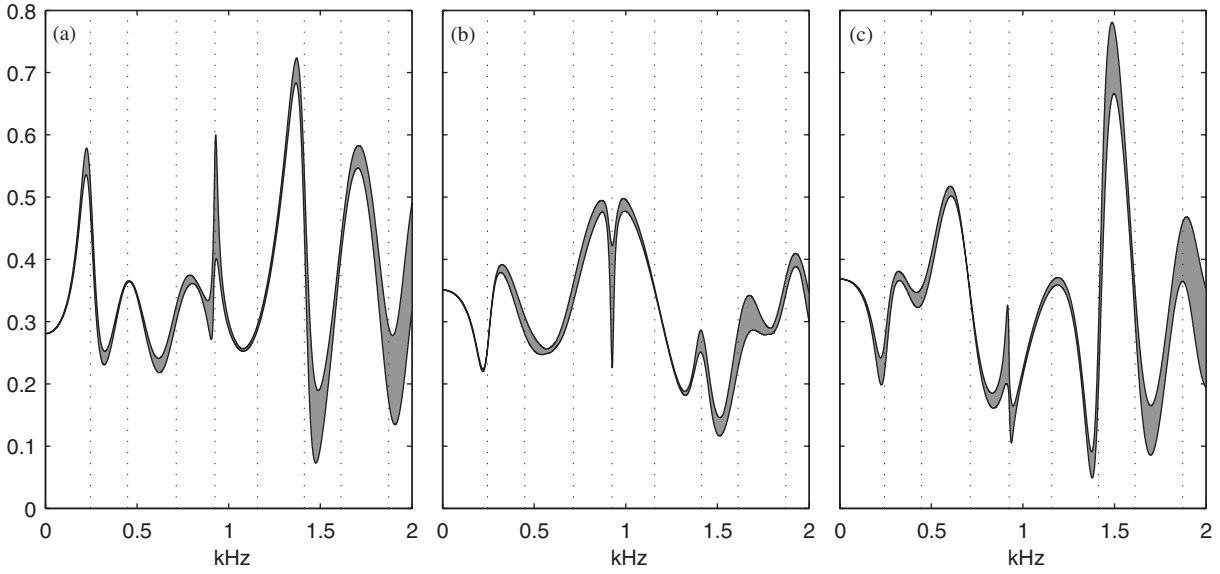

Fig. 11. Energy sharing in three-rod system under all possible variations in rod loss factors between 0.5% and 5%. The plots (a)–(c) correspond to the three rod sections. Dotted lines indicate positions of system resonant frequencies.

Table 2
Parameters of three-rod system

Rod no	Unit mass (kg/m)	Sound speed (m/s)	Length (m)	Driving point (m)	Driving force (N)
1	2	4800	4	0.8	1
2	4	3900	2.5	0.5	j
3	3	5200	3.5	0.9	$1+j$

were obtained by assuming uniform broadband excitation with the response frequency averaged in 4 bands of equal width between 0 and 2 kHz. The iso-energy lines superposed on the tone maps serve for better visualisation of main trends.

As expected, the results indicate that both the amount of damping and the damping placement play an important role in vibration control. Firstly, a saturation effect takes place, seen from the rising spacing between iso-energy lines. Increase in damping is most effective when the initial damping is very low; by adding more and more damping the control effect loses efficiency. This is self-explanatory: damping controls resonances, the role of which in the overall response diminishes as damping increases. The near-horizontal iso-energy lines of beam energy plots show that the principal effect on beam vibration is produced by the beam's own damping. The analogous result applies to the plate only at low frequencies where the iso-lines are almost vertical. At medium and higher frequencies the plate is equally controlled by the beam damping as by its own damping. Finally, the overall vibration is more sensitive to beam damping than that of the plate.

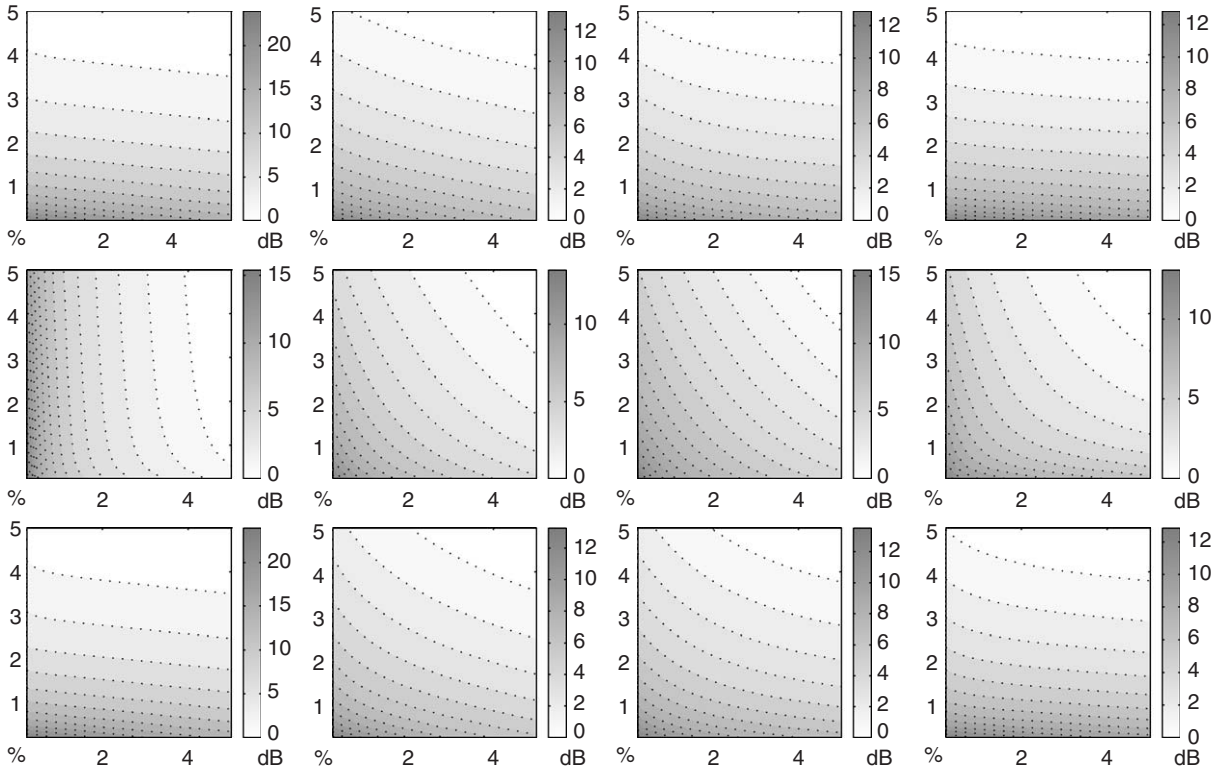

Fig. 12. Normalised, frequency-averaged, kinetic energy level of beam–plate system in dependence of damping. Top row, beam energy; middle row, plate energy; bottom row, global kinetic energy. The averaging bands: 1st column 0–500 Hz; 2nd column 500–1000 Hz; 3rd column 1000–1500 Hz; 4th column 1500–2000 Hz. Abscissa, plate loss factor in %, ordinate, beam loss factor in %. Dotted iso-lines are spaced by 1 dB.

The last conclusions are not generally applicable to arbitrary coupled sub-systems, but rather to the cases represented by the currently analysed system, i.e. to strongly coupled sub-systems only one of which is driven, moreover by broadband excitation. A simplified, yet scrupulous, modelling of such sub-systems via generic structural properties, e.g. as done in Ref. [7], will most likely be sufficient to provide the same type of conclusions.

4. Energy density and energy flow

4.1. Independence of axial and flexural flows

In a straight beam vibrating in accordance with thin-rod and Euler–Bernoulli models the energies carried by axial and flexural movements can be taken as independent. The kinetic energy density i.e. the energy per unit beam length can be found to be

$$e_{\mathrm{kin}} = \int_s \rho \left\langle \left| u(t) \right|^2 \right\rangle \mathrm{d}S = \frac{m'}{2} \left[\left\langle \dot{u}_a(t)^2 \right\rangle + r^2 \left\langle \left(\frac{\partial \dot{u}_f(t)}{\partial x} \right)^2 \right\rangle + \left\langle \dot{u}_f(t)^2 \right\rangle \right], \tag{7a}$$

where S is the surface of cross-section, ρ the mass density (assumed constant over the cross section), u the particle velocity vector, m' the beam mass per unit length, r the radius of gyration of the cross-section, u_a and u_f are the displacements of longitudinal and flexural vibrations. The middle term originates from the axial motions induced by flexure. It is typically much smaller than the third term which represents the main contribution by flexure. In harmonic motion the spatial differentiation of u_f corresponds to the multiplication by flexural wavenumber k_f. This makes the second term differ from the third one by an order of magnitude of $(rk_f)^2$. Since rk_f has to stay well below unity to make the Euler–Bernoulli theory applicable, the second term will be negligible in comparison with the third term. In the rest of the paper the kinetic energy density will be considered as a sum of two components: an axial one, corresponding to the first term, and a flexural one corresponding to the third term.

Potential energy density originates from axial motions only; it reads

$$e_{\text{pot}} = \int_s \langle \sigma(t)\varepsilon(t) \rangle \, \mathrm{d}S = \frac{ES}{2} \left[\left\langle \left(\frac{\partial u_a(t)}{\partial x} \right)^2 \right\rangle + r^2 \left\langle \left(\frac{\partial^2 u_f(t)}{\partial x^2} \right)^2 \right\rangle \right], \tag{7b}$$

where σ and ε are the axial stress and strain and E the Young's modulus. The division of potential energy to one axial and one flexural component is self-explanatory.

An analogous analysis readily shows that the energy flow through the beam can be split into two parts: one induced by longitudinal vibration, the other by flexural vibration. In conclusion, the energy densities and the energy flow of longitudinal and flexural vibration can be considered as de-coupled and can be treated separately.

4.2. Energy flow and density

Energy density and energy flow are local variables, functions of observation position. In order to show a function of two variables, position and frequency, in a simple but meaningful way a grey tone map will be used. The abscissa scale of each map shows the position along the beam counting from the free end. The excitation position is thus at 0.5 m, the connection position at 2 m. As the modal density of the whole system, largely dominated by the beam flexural modes, decreases with frequency the ordinate i.e. the frequency axis will be displayed in a square root scale for better visual resolution. The quantity shown on the map will be presented by grey shades in decibels. The adjacent tone scale quantifies each map. To keep the maps clear the presented quantity will be truncated to some lower value in order to restrain the dB dynamics. This means that all the values equal to or below the truncation threshold will be presented in the same tone—black. The position of system resonant frequencies is indicated by small circles along the right-hand side vertical axis.

Fig. 13 shows the maps of total energy density (a) and energy flow (b) in the beam. The excitation position at 0.5 m is clearly identifiable. The objective is to emphasise spatial rather than frequency variations. Since energy variation with frequency is large, the energy map is normalised by the space-averaged energy density. Thus at each given frequency the values of energy density along the beam are divided by the mean spatial energy density at this frequency, making the average value of each frequency line equal to unity. The energy density displays a complicated pattern of lobes which narrow with frequency increase. Such lobes, two per wavelength, result

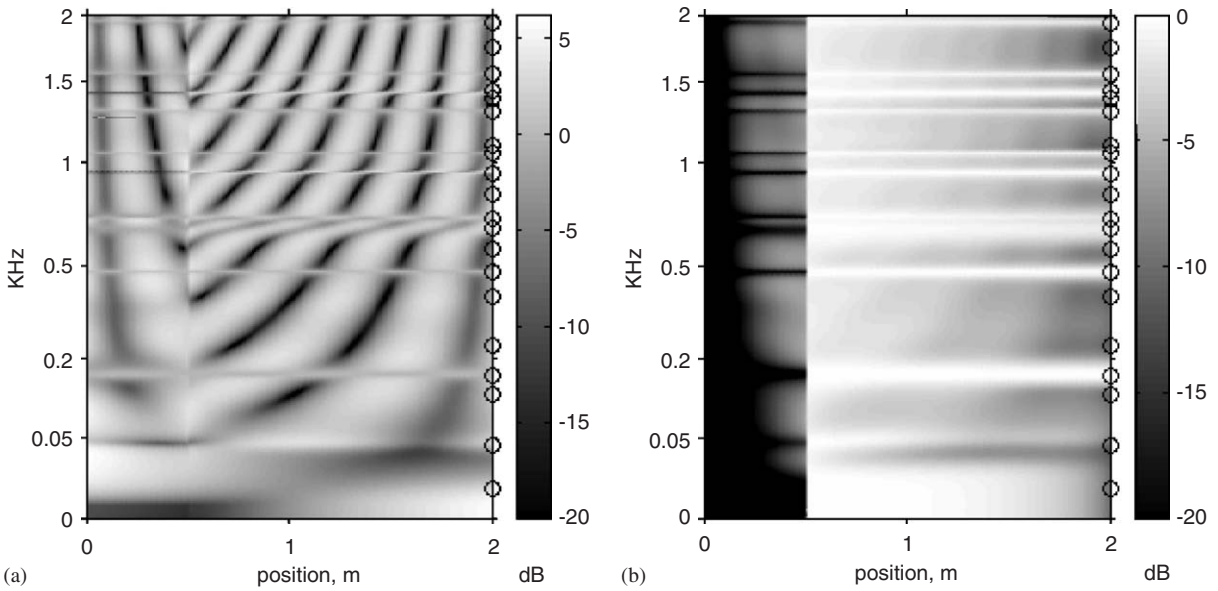

Fig. 13. Beam–plate system: (a) normalised total energy density; (b) total energy flow normalised to power input.

from the interference of vibration waves which move in opposite directions. At the frequencies where the input power is mainly transmitted to the plate, such as at 180, 480 Hz etc, the map shows horizontal bands which are not of lobar nature, i.e. which represent fairly uniform energy density distribution along the beam. The condition of large power transfer to the plate corresponds to low amplitude of reflected waves resulting in weak interference with the waves moving toward the plate. The excitation position is seen as a vertical line representing a discontinuity in energy density. It will be seen that this discontinuity is caused by the potential energy density exhibiting a jump at the excitation point. The maxima of normalised energy density are around 7 dB, i.e. about 5 times the average value.

The energy flow map shown on Fig. 13(b) is also normalised, this time by the net input power. At the excitation point the input power is split into two components: one directed to the plate, the other directed to the free end. These two components are of opposite sign, but in order to fit the decibel scale both are presented as positive. The frequency regions of strong transmission to the plate are easily recognised as white bands stretching from the excitation position to the right. While in some frequency bands the power transmission to the plate is strong, in other bands is poor. The injected power in these bands is thus mostly consumed by the beam. Such a local energy consumption is often disregarded, especially in measurements of energy flow.

The energy flow of axial and flexural motion are separately presented in Fig. 14. In the beam section spanning between the free end and the excitation point the energy flow is always directed towards the free end. The conversion of waves impinging the free end cannot take place which makes the flow negative throughout this section for both axial and flexural vibration. The areas of negative flow in the section spanning from the excitation to connection points are marked by "–" symbol. The lines of separation of negative and positive energy flow are always visible. By increasing frequency the bands of positive and negative energy flow of a particular type of motion,

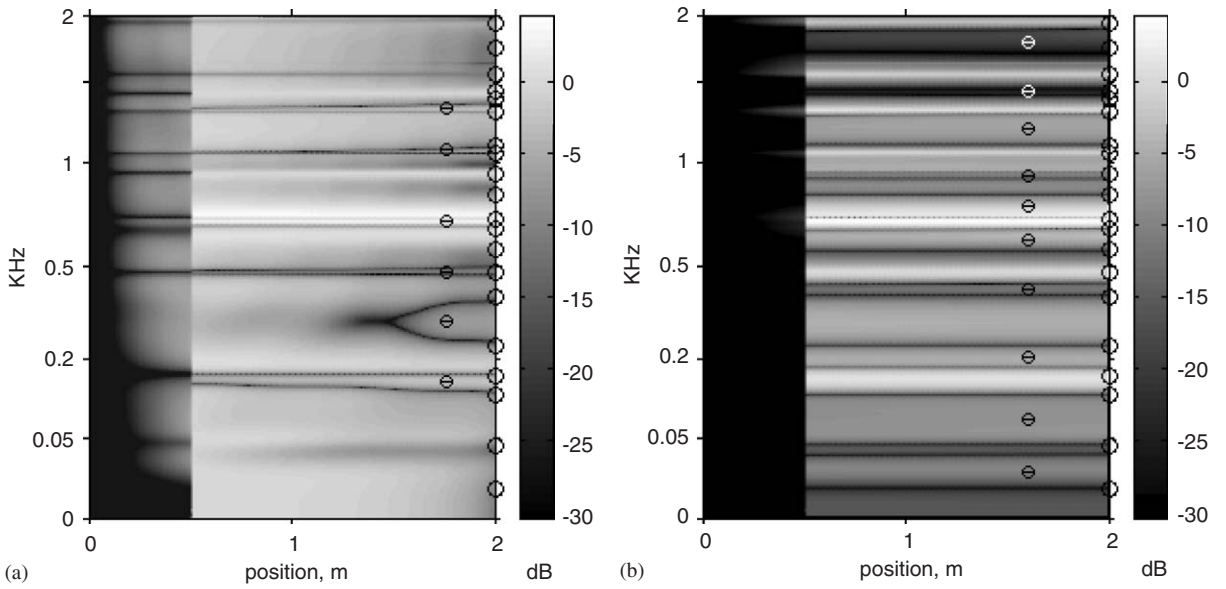

Fig. 14. Beam–plate system. Flexural (a) and axial (b) values of energy flow normalised to unit input power. Markers "–" indicate areas of negative flow. The flow values from 0 m (free end) to 0.5 m (excitation point) are negative throughout and are not marked as such.

flexural or axial, alternate. In the example analysed the axial energy flow regularly changes direction as the frequency increases. Since the wavelength of axial motion are large, which does not allow sufficient flow drop across the beam section between the excitation and connection points, the axial flow at a given frequency is as a rule either completely positive or completely negative. This is not the case with flow of flexural vibration: the frequency band of negative flow at the connection point narrows by approaching the driving point. In a band between approx. 250 and 350 Hz the flow is positive at the side of driving point and negative at the opposite side, i.e. at both the excitation and connection points the flexural power enters the beam to be dissipated in its interior. The power entering the beam from the plate side is fed by the conversion of axial vibration arriving to the plate. The total energy flow is always directed toward the plate, thus any negative flow of one type of vibration, either axial or flexural, will be always accompanied by a stronger flow of the other type of vibration. This explains the existence of levels higher than 0 dB of the normalised flow at some frequency bands. The partial flow of either axial or flexural vibrations can occasionally be of a higher level than the total flow.

Fig. 15 shows the density maps of kinetic and potential energies of flexural vibration. The two energies are distributed in a similar way away from the beam ends and the driving point but in the vicinity of these singularities any similarity is lost. The potential energy density shows a strong discontinuity at the driving position, discussed already in Ref. [1]. This energy density is proportional to the net value of energy flow divergence. The map indicates that the net divergence oscillates considerably along the beam implying that some sections absorb a lot more energy than other. This phenomenon may have considerable importance in optimising the placement of vibration absorption treatments.

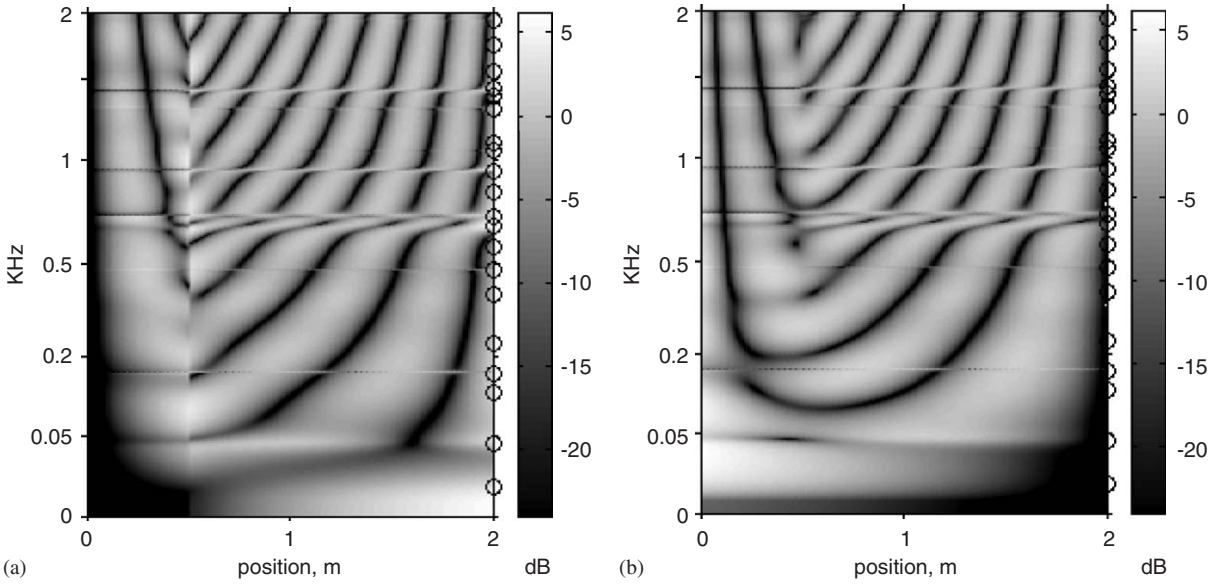

Fig. 15. Beam–plate system. Kinetic (a) and potential (b) normalised energy density of flexural motion. Circles indicate system resonant frequencies.

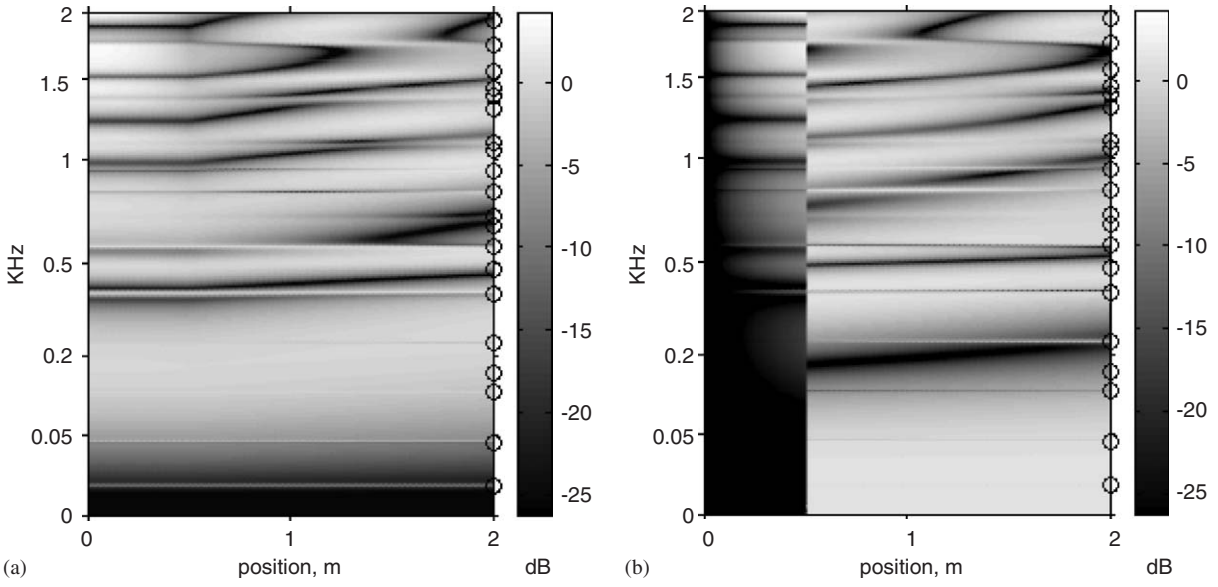

Fig. 16. Beam–plate system. Kinetic (a) and potential (b) normalised energy density of axial motion. Circles indicate system resonant frequencies.

The maps of kinetic and potential energy densities of axial motion, Fig. 16, show that significant spatial variations of two energies start only at high frequencies, above 1 kHz, at which the beam length becomes comparable to half the axial wavelength. At lower frequencies the beam

is vibrating axially almost as a rigid mass, producing a uniform distribution of energy density. The kinetic and potential energy densities give dissimilar spatial-frequency pattern at all positions, even away from discontinuities. The total energy density of axial vibration varies very little along the beam, implying that the high values of kinetic energy density are accompanied by low values of potential energy density and vice versa.

Maps in Fig. 15 show that the locations of high potential energy density can often be identified experimentally in an easy way. It is sufficient to measure the vibration level, i.e. the kinetic energy density. In the case of axial vibration the positions of high potential energy will coincide with vibration level minimum at most positions. In the case of flexural vibration, the two energies will match away from discontinuities. Near the boundaries within the distance of half the wavelength the two energies may be very different, depending on the type of boundary. Close to the excitation the situation may vary a lot in dependence of the excitation type; no general rule can be given here.

5. The role of damping in experimental energy characterisation

Various techniques allow measurement of energy in rods and beams. Perhaps the most versatile of these techniques, the wave separation technique, consists of extracting the amplitudes of vibration waves from measured data and inserting these values in the governing formulae for energy and energy flow expressed in terms of wave amplitudes. As a rule the separation is done by neglecting structural damping, believed to produce negligible effects on results. This section investigates how the neglecting of damping affects two known applications of experimental vibration energy techniques: measurement of energy flow and measurement of energy coefficients of joints.

5.1. Measurement of energy flow

The analysis will be carried out by assuming that the wave separation technique is used, [10–12]. The wave amplitudes are computed from axial and flexural vibration data sampled at different points along the beam. As the objective here is to analyse the effect of neglecting damping, it will be assumed that the vibration measurements are error free.

The general relationship between the known velocities at the sampling points and unknown wave amplitudes reads:

$$\mathbf{v} = \mathbf{X}\mathbf{A} \tag{8}$$

where $\mathbf{v}$ is the N-vector of velocities at measurement points, $\mathbf{A}$ the M-vector of wave amplitudes and $\mathbf{X}$ the $N \times M$ matrix of wave coefficients relative to the measurement points. This matrix contain the well known terms of the form $e^{\pm jkx}$ which represent a general solution to wave motion of the beam, k being a complex wavenumber. Axial vibration of beam consists of two waves ($M = 2$) while flexural vibration consists of four waves ($M = 4$). If $N = M$ the amplitude vector is obtained by inversion, if $N > M$ it is obtained by suitable pseudo-inversion. The structural damping is contained in k, i.e. in the matrix $\mathbf{X}$ which is supposed to be known.

Neglecting structural damping will yield two types of error: (1) the values of extracted amplitudes of wave motion will be inaccurate (2) by inserting the amplitude values into the equations of energy density and energy flow which do not take damping into account another error is committed. This error would have occurred even if the values of wave amplitudes were exact.

A concrete error analysis has been done for the current beam–plate system. Several combinations of vibration sampling points were employed. For each combination the wave amplitudes of axial and flexural vibrations were computed, first exactly and then by setting damping to zero. The computed values of wave amplitudes, exact and contaminated, were then fed into the equations of energy density and energy flow given in Ref. [1], in the latter case by setting again damping to zero. The whole procedure represents in fact two virtual measurements, one performed by taking damping into account, the other performed by neglecting it.

Four equidistant sampling points were used for extraction of flexural wave amplitudes. Two inner points of the same array were used for the extraction of axial wave amplitudes. Results are shown for three configuration of sampling points: (a) spaced by 30 cm starting from the position 0.8 m, (b) spaced by 10 cm starting from 1.1 m, (c) spaced by 10 cm starting from 0.55 m. Results refer to the middle position of the array: those of configurations (a) and (b) refer to the position 1.25 m, those of configuration (c) to the position 0.7 m (20 cm away of the excitation point).

The error in evaluating energy density from data contaminated by neglecting damping was found negligible. This error was found high only in frequency regions close to the coincidence frequencies, i.e. frequencies at which the spacing between measurement points matches an integer multiplier of half the wavelength. At the coincidence frequencies the matrix of wave coefficients becomes singular so that even a small error in the coefficients close to a coincidence frequency will produce large error in the result. This effect is not an exclusive consequence of using incorrect damping values. In real measurements it is contributed by all sources of error, such as error in positioning of the sampling points, phase error between signals, etc. However, neglecting the damping is the only source of error, in the present simulation.

The error in evaluating energy flow was found not negligible. Fig. 17 shows the relative error in the evaluation of energy flow by neglecting damping. The relative error is defined as the ratio of the difference of the erroneous and exact values and the exact value. The bold line denotes the real part of flow, the thin line the imaginary part. Dotted lines mark system resonant frequencies. Square root scales are applied to both abscissa and ordinate to improve visual resolution.

At some frequencies the error of neglecting damping becomes extremely high. This is the case especially in the vicinity of frequencies at which the flow changes direction. Close to such ''flow reversal'' frequencies the value of the flow is small and changes rapidly. By setting the damping to zero the flow reversal frequencies will be shifted with respect to the exact ones which explains the extreme values of error found. It can be seen that the error has not any discernible behaviour close to resonance frequencies. It can be further seen that the error in net energy flow decreases by decreasing the spacing between the sampling points. The error in the imaginary flow is not very sensitive to the spacing. The exception regarding the sensitivity of net flow to the spacing is noticeable at low frequencies: the error becomes insensitive to the spacing and converges to -1 with the frequency approaching zero. Thus at low frequencies neglecting damping leads to a major underestimation of net energy flow. By analysing the expressions for energy flow in Ref. [1] it can be shown that at low frequencies the contribution of the evanescent waves to net energy

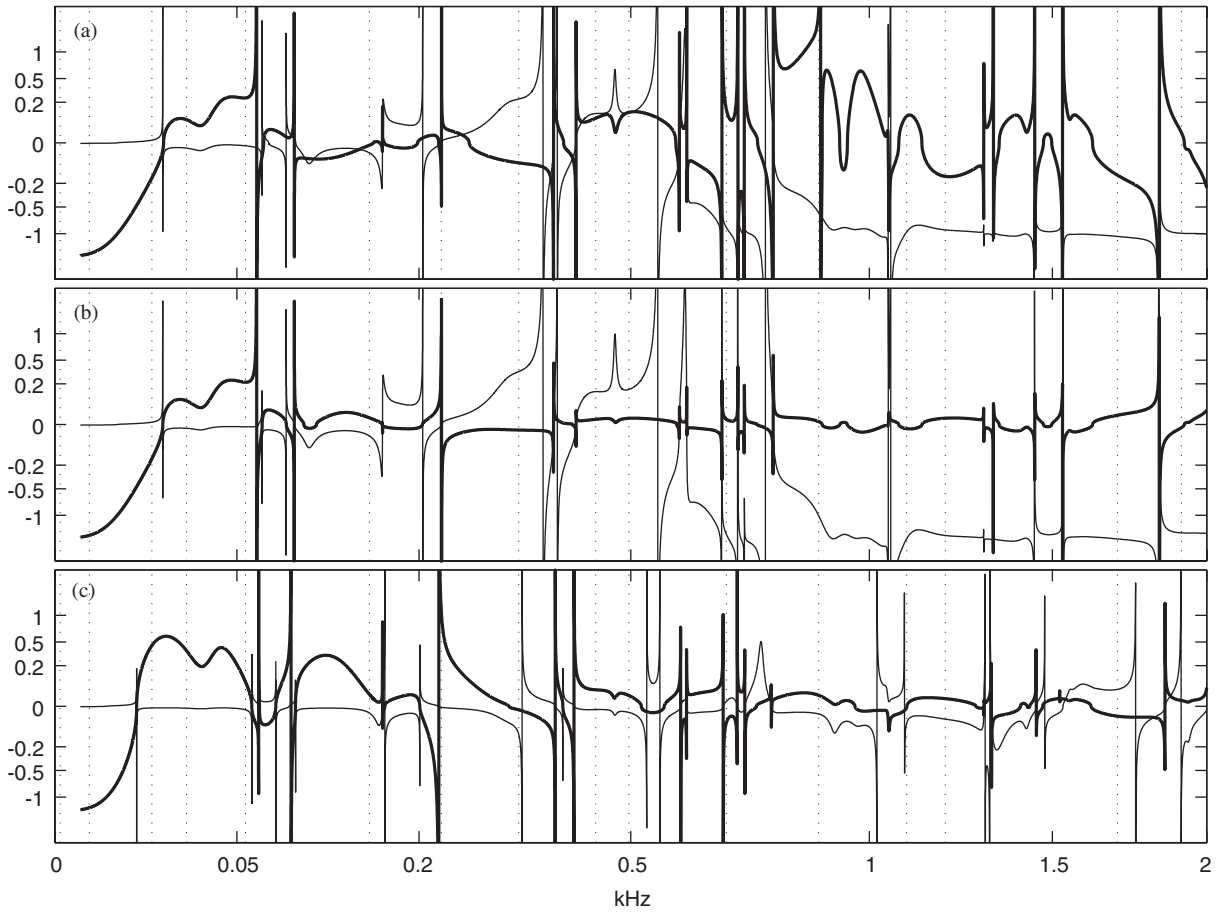

Fig. 17. Relative error in the evaluation of flexural energy flow in a beam using wave decomposition technique. Bold line, real part of flow; thin line, imaginary part. Transducer spacing, top 0.3 m; middle and bottom 0.1 m; array centre from nearest discontinuity, top and middle 0.75 m, bottom 0.2 m. Dots indicate system resonant frequencies. Most of the error maxima occur at frequencies at which energy flow change sign.

flow becomes not negligible while the contaminated data modify this contribution a lot, much more than other contributions. The axial vibrations do not contain evanescent waves, thus the low-frequency error (not shown) is small.

5.2. Measurement of joint energy coefficients

The existence of damping will affect the classical way the reflection and transmission of vibration waves is analysed. The two phenomena are most often expressed by energy indicators. If a rod or a beam exhibits a jump of mechanical properties, such as caused by a joint or change in cross section, one part of incident energy carried by vibration will be reflected and one part will be transmitted. If the discontinuity is not conservative, the following simple energy equilibrium rule applies:

$$r + t + a = 1, \tag{9}$$

where r, t and a stand for reflection, transmission and absorption energy coefficients due to the discontinuity. These coefficients can be expressed in terms of vibration wave amplitudes at the discontinuity. It will be shown that the presence of damping in the rod affects the reading of energy coefficients.

Let a longitudinal wave in a rod strike a discontinuity with an amplitude A (complex). As a result, a reflected wave of complex amplitude R and a transmitted wave of complex amplitude T are generated. The discontinuity is taken to be at the origin, $x = 0$. The net energy flow impinging the discontinuity reads, [1], (A6):

$$\mathrm{Re}(\bar{P})_1 = \tfrac{1}{2}\sqrt{E_1 m_1'}\omega^2 |A^2| \left[1 - |\alpha^2| + \eta \mathrm{Im}\{\alpha\}\right], \tag{10a}$$

where $\alpha = R/A$ is the complex ratio of the reflected and incident amplitudes while the subscript 1 refers to the upstream part of the rod. At the other side of discontinuity only the transmitted wave is assumed to exist making the energy flow carried across the discontinuity equal to

$$\mathrm{Re}(\bar{P})_2 = \tfrac{1}{2}\sqrt{E_2 m_2'}\omega^2 |A^2||\tau^2| \tag{10b}$$

with $\tau = T/A$. The incident energy flow $\mathrm{Re}\{\bar{P}\}_0$ is obtained by setting $\alpha = 0$. Consequently, the energy coefficients read

$$r = 1 - \frac{\mathrm{Re}(\bar{P})_1}{\mathrm{Re}(\bar{P})_0} = |\alpha^2| - \eta \mathrm{Im}\{\alpha\}, \quad t = \frac{\mathrm{Re}(\bar{P})_2}{\mathrm{Re}(\bar{P})_0} = \sqrt{\frac{E_2 m_2'}{E_1 m_1'}}|\tau^2| \tag{11}$$

The reflection coefficient is thus seen to not merely be the absolute square of the reflected/incident amplitude ratio but depends in addition on the damping in the upstream part of the rod. By ignoring damping an error is produced which will be illustrated by the following example.

Assume the rod has a discontinuity in the form of a linear axial joint. The joint is characterised by its complex mobility matrix $\mathbf{M}$ defined at two terminal points 1 and 2 by

$$\begin{Bmatrix} \dot{u}_1 \\ \dot{u}_2 \end{Bmatrix} = \mathbf{M} \begin{Bmatrix} F_1 \\ F_2 \end{Bmatrix}, \quad \mathbf{M} = \begin{bmatrix} M_{11} & M_{12} \\ M_{21} & M_{22} \end{bmatrix}.$$

Reciprocity implies $M_{12} = M_{21} = M_t$. Recalling the strain–stress relationship for pure axial motion and assuming the terminal forces and velocities as positive if directed into the joint, the amplitude ratios α and τ can be readily evaluated (proof omitted for the sake of brevity):

$$\alpha = 1 - 2\frac{1 + \kappa_2 M_{22}}{D}, \quad \tau = -2\frac{\kappa_1 M_t}{D} \tag{12}$$

with

$$\kappa = \sqrt{E\rho}(1 + \mathrm{j}\eta/2), \quad D = (1 + \kappa_1 M_{11})(1 + \kappa_2 M_{22}) - \kappa_1 \kappa_2 M_t^2. \tag{12a}$$

By analysing Eq. (12) it can be seen that even joints which are dissipation free (M purely imaginary) will yield reflection coefficient dependent on rod damping via the complex factors κ.

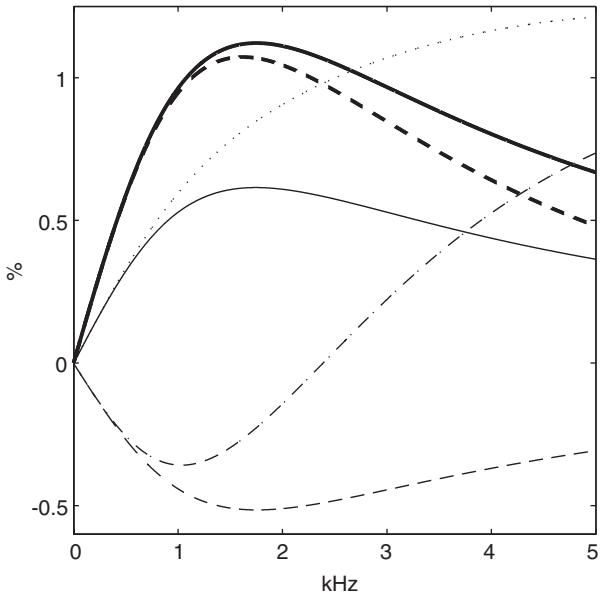

Fig. 18. Absorption coefficient of a lossy mass–spring joint in a rod established via wave energy flow computation. Thick line, exact value; thin line, approximate value by neglecting damping in the rod. Full lines, normal joint orientation; dotted lines, reversed joint orientation. Dashed and dashed-dotted line, approximate value for a lossless joint, normal and reversed orientations, respectively.

To get some concrete insight into the nature of error caused by neglecting the rod losses it will be assumed that the joint is a simple system consisting of a spring of stiffness ζ and loss factor η_j followed by a mass m. The joint mobility matrix then reads:

$$M = \frac{1}{\mathrm{j}\omega m}\begin{bmatrix} 1-\omega^2 m/\zeta & -1 \\ -1 & 1 \end{bmatrix}, \qquad \zeta = \mathrm{Re}\{\zeta\}(1+\mathrm{j}\eta_j).$$

The rod will be taken of the same material and unit mass as in the beam–plate case. The joint parameters are: $m = 0.2\,\mathrm{kg}$, $\zeta = 5\times 10^7\,\mathrm{N/m}$, $\eta_j = 1\%$. Fig. 18 shows the absorption coefficient of the joint computed exactly and by neglecting the damping in the rod, (11). Both joint orientations are considered: the direct one (mass followed by the spring) and the reverse one. The latter is obtained by interchanging the position of the diagonal terms in the mobility matrix. The dashed and dashed-dotted curves shown on the same plot represent the case when the joint damping is set to zero while neglecting the damping in the rod.

The relative error by neglecting the damping is seen to be very large. In particular, the reflection and transmission coefficients of an undamped joint will not add to unity which may result even in negative absorption as seen in Fig. 18.

An analogous situation applies to flexural vibration in a beam. In this case the evanescent waves will affect the energy coefficients in addition to propagating ones. The formulae for the reflection and transmission energy coefficients become increasingly complex as the damping couples the evanescent and propagating waves in energy flow.

For example, when a propagating wave impinges a discontinuity, it will create one reflected pair of propagating and evanescent waves and one transmitted pair of such waves. By introducing the symbols β for the ratio between the reflected evanescent wave and the incident wave and γ for the ratio between the transmitted evanescent wave and the incident wave, the two energy coefficients can be found from energy flow equations of [1, (B3b)]:

$$r = 1 - \frac{\mathrm{Re}(\bar{P})_1}{\mathrm{Re}(\bar{P})_0} = |\alpha^2| + \frac{\eta}{2}\left[\mathrm{Im}\{\alpha\} + \frac{|\beta^2|}{2} - \mathrm{Re}\{(1+\alpha)\beta^*\} + \mathrm{Im}\{(1-\alpha)\beta^*\}\right],$$

$$t = \frac{\mathrm{Re}(\bar{P})_2}{\mathrm{Re}(\bar{P})_0} = \sqrt[4]{\frac{B_2 m_2'^3}{B_1 m_1'^3}}\left\{|\tau^2| + \frac{\eta}{2}\left[\frac{|\beta^2|}{2} - \mathrm{Re}\{\beta\gamma^*\} - \mathrm{Im}\{\beta\gamma^*\}\right]\right\}, \tag{13}$$

where the asterisk stands for complex conjugate. It can be seen that the own beam damping plays again a major role in the computation of energy coefficients of a beam joint.

6. Concluding remarks

The computational study of a beam attached to a plate, while treating not more than a particular case, has nevertheless demonstrated some characteristic features of energy distribution in beams (rods) which, by their nature, can be considered as being generic. The main points emanating from this study can be summarised as follows:

- Axial vibrations of a realistically excited beam may be of the same importance with respect to energy flow as flexural vibrations. In particular these vibrations may act as a "hidden" carrier of energy to the surrounding sub-systems.
- Due to wave conversion which can take place at beam discontinuities the energy flow in the beam due either to axial or flexural vibrations can become negative even if the only vibration source is at the beam itself.
- While the frequency-averaged input net power to a system is fairly independent of damping, the energy consumed by a beam, i.e. the sum of energy flows exchanged via excitation and connection points, will depend crucially on damping.
- In a beam-driven built-up system the sharing of energy between the beam and the rest of the system is little dependent on damping providing the coupling is strong.
- Beam damping plays a major role in the experimental evaluation of energy flow and energy indicators of the beam. However, the evaluation of energy density is not affected by damping.
- Computation of absorption, reflection and transmission coefficients at a beam discontinuity or an incorporated joint will be erroneous if the beam damping is neglected.

Appendix. Model of beam and plate vibration

In a straight beam the axial and lateral motions are uncoupled. The axial, lateral and angular displacements of the beam at point B—u_B, u_B, u_B—and forces and moments at point A—N_A, F_A,

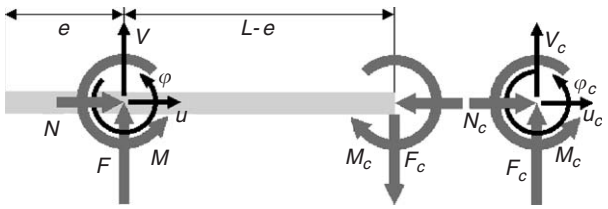

Fig. A1. Beam–plate model.

M_A—can be linked by a 3×3 mobility matrix:

$$\mathbf{q}_B = \frac{1}{\mathrm{j}\omega}\Lambda_{BA}\mathbf{Q}_A, \quad \mathbf{q}_B = \begin{Bmatrix} u_B \\ v_B \\ w_B \end{Bmatrix}, \quad \mathbf{Q}_A = \begin{Bmatrix} N_A \\ F_A \\ M_A \end{Bmatrix}, \quad \mathbf{\Lambda}_{BA} = \begin{bmatrix} Y_{BA} & 0 & 0 \\ 0 & H_{BA} & S_{BA} \\ 0 & G_{BA} & K_{BA} \end{bmatrix}. \tag{A.1}$$

Fig. A1 represents the model of the beam–plate system. The total vibration load acting on the beam consists of the external load at the excitation point E and an internal load acting at the connection point C. The latter acts also on the plate but in opposite direction as seen on Fig. A1.

The plate moment mobilities depend on the orientation of the excitation which follows from Fig. 1. The symbols for mobilities of the plate will be taken the same as for the beam; a superscript "b" or "p" will distinguish between the two. With such a convention in mind, the governing continuity equations of the velocities at the connection point can be written as

$$\begin{aligned} \text{axial}: \; & Y^b_{CE}N - Y^b_{CC}N_c = H^p_{CC}N_c + S^p_{CC}M_c, \\ \text{lateral}: \; & H^b_{CE}F - H^b_{CC}F_c + S^b_{CE}M - S^b_{CC}M_c = Y^p_{CC}F_c, \\ \text{angular}: \; & G^b_{CE}F - G^b_{CC}F_c + K^b_{CE}M - K^b_{CC}M_c = G^p_{CC}N_c + K^p_{CC}M_c. \end{aligned} \tag{A.2}$$

By denoting the column of external load by $\mathbf{Q}_E$ and that of internal load by $\mathbf{Q}_C$, the following solution is obtained for the latter from (A.2) and (A.1):

$$\mathbf{Q}_C = \mathbf{\Gamma}^{-1}\mathbf{\Lambda}^b_{CE}\mathbf{Q}_E, \quad \mathbf{\Gamma} = \begin{bmatrix} (Y^b_{CC} + H^p_{CC}) & 0 & S^p_{CC} \\ 0 & (H^b_{CC} + Y^p_{CC}) & S^b_{CC} \\ G^p_{CC} & G^b_{CC} & (K^b_{CC} + K^p_{CC}) \end{bmatrix}. \tag{A.3}$$

The matrix $\mathbf{\Gamma}$ clearly represents the coupling effect between the beam and the plate. It depends only on the mobilities of the two structures at the coupling point. In the absence of the plate the related plate mobilities become infinite and thus $\mathbf{Q}_C$ becomes zero.

Once the reaction load $\mathbf{Q}_C$ is known, the response velocities at an arbitrary point X can be obtained by the superposition of external and internal loads using the notation of (A.1):

$$\mathbf{q}_X = \frac{1}{\mathrm{j}\omega}(\mathbf{\Lambda}_{XE}\mathbf{Q}_E - \mathbf{\Lambda}_{XC}\mathbf{Q}_C) = \mathbf{\Xi}_{XE}\mathbf{Q}_E, \quad \mathbf{\Xi}_{XE} = \frac{1}{\mathrm{j}\omega}(\mathbf{\Lambda}_{XE} - \mathbf{\Lambda}_{XC}\mathbf{\Gamma}^{-1}\mathbf{\Lambda}^b_{CE}). \tag{A.4}$$

The complex 3×3 displacement transfer matrix $\boldsymbol{\Xi}$ represents the liaison between the external load vector $\mathbf{Q}_E$ at the position E and the displacement response vector $\mathbf{q}_X$ at an arbitrary position X. This matrix will be further used to compute the amplitudes of vibration waves in the beam.

The wave amplitudes are not unique for the whole beam. Excitation point represents a discontinuity which splits the beam into two sections, each of which will have its own set of wave amplitudes. To compute these amplitudes 3 points will be identified which limit the two sections: free end point O ($x = 0$), excitation point E ($x = e$) and connection point C ($x = L$).

The displacement amplitudes of longitudinal and flexural vibration, U and V, given in terms of wave amplitudes read:

$$U = U_+ \mathrm{e}^{-\mathrm{j}k_l x} + U_- \mathrm{e}^{\mathrm{j}k_l x}, \quad V = A_+ \mathrm{e}^{-\mathrm{j}k_f x} + A_- \mathrm{e}^{\mathrm{j}k_f x} + C_+ \mathrm{e}^{-\mathrm{j}k_f x} + C_- \mathrm{e}^{\mathrm{j}k_f x}. \tag{A.5}$$

The amplitudes at each beam section will be arranged in a 6-column complex vector $\mathbf{A}$:

$$\mathbf{A} = \begin{Bmatrix} U_+ \\ U_- \\ A_+ \\ A_- \\ C_+ \\ C_- \end{Bmatrix}. \tag{A.6}$$

The amplitude vector of a given section can be recovered from the known displacement vectors at any two different points within the section concerned. By denoting the two points by A and B and using Eqs. (A.4) and (A.5) the amplitude vector $\mathbf{A}$ can be expressed in terms of the excitation vector $\mathbf{Q}_E$:

$$\mathbf{A} = \boldsymbol{\Psi}_{AB,E} \mathbf{Q}_E, \tag{A.7}$$

where $\boldsymbol{\Psi}$ is the 6×3 amplitude conversion matrix relative to points A and B which gives the vector $\mathbf{A}$ directly in terms of the external loading $\mathbf{Q}_E$:

$$\boldsymbol{\Psi}_{AB,E} = \boldsymbol{\Omega}_{AB}^{-1} \begin{Bmatrix} \boldsymbol{\Xi}_{AE} \\ \boldsymbol{\Xi}_{BE} \end{Bmatrix}, \quad \boldsymbol{\Omega}_{AB} = \begin{bmatrix} \mathrm{e}^{-\mathrm{j}y_A} & \mathrm{e}^{\mathrm{j}y_A} & 0 & 0 & 0 & 0 \\ 0 & 0 & \mathrm{e}^{-\mathrm{j}z_A} & \mathrm{e}^{\mathrm{j}z_A} & \mathrm{e}^{-z_A} & \mathrm{e}^{z_A} \\ 0 & 0 & -\mathrm{j}k_f \mathrm{e}^{-\mathrm{j}z_A} & \mathrm{j}k_f \mathrm{e}^{\mathrm{j}z_A} & -k_f \mathrm{e}^{-z_A} & k_f \mathrm{e}^{z_A} \\ \mathrm{e}^{-\mathrm{j}y_B} & \mathrm{e}^{-\mathrm{j}y_B} & 0 & 0 & 0 & 0 \\ 0 & 0 & \mathrm{e}^{-\mathrm{j}z_B} & \mathrm{e}^{\mathrm{j}z_B} & \mathrm{e}^{-z_B} & \mathrm{e}^{z_B} \\ 0 & 0 & -\mathrm{j}k_f \mathrm{e}^{-\mathrm{j}z_B} & \mathrm{j}k_f \mathrm{e}^{\mathrm{j}z_B} & -k_f \mathrm{e}^{-z_B} & k_f \mathrm{e}^{z_B} \end{bmatrix}. \tag{A.7a}$$

The wave amplitudes of the section between the free end and the excitation point, will be thus obtained using the conversion matrix $\boldsymbol{\Psi}_{OE,E}$, those of the section between the excitation point and the plate using $\boldsymbol{\Psi}_{EC,E}$. Once the wave amplitudes are computed, the energy density and energy flow in the beam become available using the expressions given in Ref. [1].

References

[1] G. Pavić, Vibration damping, energy and energy flow in rods and beams: governing formulae and semi-infinite systems, *Journal of Sound and Vibration*, 2006, in press (doi:10.1016/j.jsv.2005.07.021).
[2] E. Skudrzyk, *Simple and Complex Vibratory Systems*, Pennsylvania State University Press, University Park, 1968.
[3] A.S. Nikiforov, Impedance of an infinite plate with respect to a force acting in its plane, *Akustichesky Zhurnal* 14 (1968) 297–298 (in Russian).
[4] L. Cremer, M. Heckl, E.E. Ungar, *Structure-Borne Sound*, Springer, Berlin, 1973.
[5] A.J. Keane, W.G. Price, A note on the power flowing between two conservatively coupled multi-modal subsystems, *Journal of Sound and Vibration* 144 (1991) 185–196.
[6] R. Langley, On the power input to point loaded hysteretically damped structures, *Journal of Sound and Vibration* 181 (1995) 657–672.
[7] B. Mace, Power flow between two continuous one-dimensional subsystems: a wave solution, *Journal of Sound and Vibration* 154 (1992) 289–319.
[8] B. Mace, The statistics of power flow between two continuous one-dimensional subsystems, *Journal of Sound and Vibration* 154 (1992) 321–341.
[9] G. Pavić, The role of damping on energy and power in vibrating systems, *Journal of Sound and Vibration* 281 (2005) 45–71.
[10] G. Pavić, Vibroacoustical energy flow through straight pipes, *Journal of Sound and Vibration* 154 (1992) 411–429.
[11] C.R. Halkyard, B.R. Mace, A wave component approach to structural intensity in beams, *Proceedings of the fourth International Congress on Intensity Techniques*, Senlis, August–September 1993, pp. 183–190.
[12] G. Pavić, Accuracy of energy flow measurement in pipes using the wave de-composition technique, *Proceedings of the fourth International Congress on Intensity Techniques*, Senlis, August–September 1993, pp. 191–198.